

Griffiths phase, magnetic memory and ac susceptibility of an antiferromagnetic titanate-based perovskite $\text{Er}_{0.9}\text{Sr}_{0.1}\text{Ti}_{0.975}\text{Cr}_{0.025}\text{O}_3$ system

R Hamdi^{1,2} , M Smari^{2,3} , A Bajorek^{4,5}, L Bessais⁶ , E Dhahri² , A Samara⁷, S A Mansour⁷ and Y Haik⁸

¹ College of Health and Life Sciences, Hamad Bin Khalifa University, Qatar Foundation, Doha, Qatar

² Laboratoire de Physique Appliquée, Faculté des Sciences, Université de Sfax, B.P. 1171, Sfax 3000, Tunisia

³ CICECO, Aveiro Institute of Materials, Department of Materials and Ceramic Engineering, University of Aveiro, 3810-193 Aveiro, Portugal

⁴ A. Chelkowski Institute of Physics, University of Silesia, Uniwersytecka 4 St., 40-007, Katowice, Poland

⁵ Silesian Center for Education and Interdisciplinary Research, University of Silesia in Katowice, 75 Pułku Piechoty 1 A, 41-500 Chorzów, Poland

⁶ CMTR, ICMPE, UMR 7182 CNRS-UPEC, 2 rue Henri Dunant, F-94320 Thiais, France

⁷ Qatar Environment and Energy Research Institute, Hamad Bin Khalifa University, Qatar Foundation, Doha, Qatar

⁸ College of Science and Engineering, Hamad Bin Khalifa University, Qatar Foundation, Doha, Qatar

E-mail: rihab.hamdi.physique@gmail.com and rhamdi@hbku.edu.qa

Received 8 October 2019, revised 3 February 2020

Accepted for publication 25 February 2020

Published 2 April 2020



CrossMark

Abstract

In this study, we investigated different physical properties of $\text{Er}_{0.9}\text{Sr}_{0.1}\text{Ti}_{0.975}\text{Cr}_{0.025}\text{O}_3$ titanate prepared by a solid-state reaction that produces a cubic structure with $Fd\bar{3}m$ (227) as a space group. Zero-Field Cooled and Field Cooled measurements show a second-order antiferromagnetic transition at Neel temperature $T_N = 23$ K, and the existence of Griffiths phase at around $T_{GP} = 132$ K. This soft magnetic material depicts a magnetic memory since it ‘remembers’ its thermal history. The relative cooling power of this titanate-based sample was then measured to be around 292.27 J kg^{-1} at 5 Tesla and 400 J kg^{-1} at 6 Tesla. However, these values are lower than the RCP value reported for the most magnetic refrigerant Gd, although these results are high enough compared to different perovskite systems. Therefore, $\text{Er}_{0.9}\text{Sr}_{0.1}\text{Ti}_{0.975}\text{Cr}_{0.025}\text{O}_3$ is a very suitable, environment-friendly magnetic refrigerant.

Keywords: ErTiO_3 , Griffiths phase, magnetic memory, AC-susceptibility, magnetic refrigeration

(Some figures may appear in colour only in the online journal)

1. Introduction

Materials research that involves combining various metal elements in one structure, like in perovskite ABO_3 , is gaining great interest in the scientific community [1]. This can be in both A and B sites in an easy way. Amongst the different groups of ABO_3 structure, we studied titanate-based perovskite ATiO_3 for its basic structure, and smart and rich

properties that make it ideal for producing new materials in various research fields.

The advantage of this kind of structure is its valency and vacancy control enhancing its catalytic activity [2]. The BO_6 octahedron makes the transfer of electron and oxygen easier, leading to non-stoichiometric oxygen, making this perovskite structure a very useful catalyst for degradation of pollutants via inducing high reducibility as noted by Bradha *et al* [2]. The

A-site cations assist the stabilization of the B-site valence making the electrons of the perovskite structure more active and external energy can excite easily [3, 4]. Thus, both the BO₆ octahedron and the A-site atoms make ABO₃ structure an active oxide.

We are interested in investigating the magnetic properties of ATiO₃ materials for their wide range of applications in magnetic memory [5, 6], bolometer applications [7–9], gas sensors, magnetoresistance [10, 11], magnetic cooling [12–14], magneto-optical devices, magneto-sensor electronics, superconducting electronics, microwaves, energy conversion applications, spintronics [15, 16]; a field of science at the interface between electronics and magnetism that exploits not only the charge of the electrons but also their spin.

Magnetic properties of rare earth titanate-based perovskite oxides (Gd, Tb, Dy, Ho, Er, Tm, Yb)TiO₃ had been investigated via neutron diffraction methods as reported by Greedan *et al* [17]. Their temperature of transition ranges from 38 K to 65 K. They are rare earth dependent.

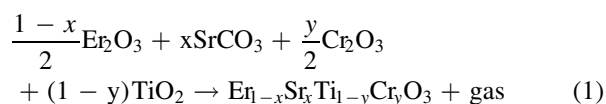
The first use of the magnetic memory effect was in ferromagnetic (FM) nanoparticles by Sun *et al* [18, 19]. After that, it had been used in different systems; isolated or interacting, systems with spin-glass state, antiferromagnetic nanoparticles, etc.

The magnetic refrigeration can be marked based on the magnetocaloric effect (MCE) by applying an external magnetic field. The gadolinium Gd is considered the most efficient magnetic refrigerant with the high value of relative cooling power (RCP) [20], which is defined as the quantity of heat transfer between cold and hot reservoirs of a thermodynamic cycle. High cost of gadolinium material is a big limiting factor, driving researchers to look for low-cost alternatives.

In this paper, we first report the synthesis of a titanate-based perovskite Er_{0.9}Sr_{0.1}Ti_{0.975}Cr_{0.025}O₃ system via solid-state reaction. Second, we present the structural and magnetic studies; magnetic memory test, ac-susceptibility measurements, and magnetocaloric study of the Er_{0.9}Sr_{0.1}Ti_{0.975}Cr_{0.025}O₃ system. We aim to study the physical properties of Er_{0.9}Sr_{0.1}Ti_{0.975}Cr_{0.025}O₃ system, especially the magnetic cooling technique based on the magnetocaloric effect.

2. Experimental method

Based on the familiar solid state reaction at high temperatures, Er_{0.9}Sr_{0.1}Ti_{0.975}Cr_{0.025}O₃ sample was prepared via combining stoichiometric amounts of Er₂O₃, SrCO₃, Cr₂O₃ and TiO₂ by following this reaction:



The used precursors were intimately ground in alcohol using agate mortar and heated repeatedly at different temperatures (900 °C/24 h; 1000 °C/24 h and 1100 °C/24 h) in Nebertherm oven in Laboratory of Applied Physics, Faculty of Sciences, University of Sfax, Tunisia, accompanied by an intermediate grinding and pressing under 5 tonnes to obtain compact pellets. The sample was then quenched in air.

We determined the structure and the phase purity of this system using x-ray diffraction (XRD) at room temperature with a scan from 10 to 100° (Cu-K_α, radiation source) using D8 Advance Bruker Diffractometer that belongs to Qatar Environment and Energy Research Institute.

The morphology and microstructure of the studied compound were investigated using a Merlin Scanning Electron Microscope (SEM) equipped with Silicon Drift Detector (SDD)-X-Max 50 from Oxford Instruments employed for the elemental analysis of the various phases which belongs to ICMPE (UMR 7182), CNRS-University Paris Est-France. Magnetic and magnetocaloric measurements were performed at both Qatar Environment and Energy Research Institute (using QD Dynacool PPMS—VSM module), and the University of Silesia, Poland (Quantum Design—MPMS).

3. Results and discussions

X-ray diffraction patterns (XRD) of Er_{0.9}Sr_{0.1}Ti_{0.975}Cr_{0.025}O₃ titanate are presented in figure 1(a). The measurement was carried out in an angular range 2θ varying from 10° to 100° at 298 K. Based on the International Centre for Diffraction Data (ICDD) database, the crystal structure of this system is cubic with Fd-3m (227) as a space group with a = 10.0772(2) Å as a lattice parameter and V = 1023.34 Å³ as a volume. It presents also erbium oxide Er₂O₃ as a second phase, as marked in the same figure, with a cubic structure (I213); a = 10.54 Å (199) and V = 1170.91 Å³. We, then, determined the crystallite size of Er_{0.9}Sr_{0.1}Ti_{0.975}Cr_{0.025}O₃ titanate which was estimated using the highest x-ray peak via Debye Scherer's formula as presented in figure 1(b):

$$D_{\text{XRD}} = \frac{k\lambda_{\text{Cu}}}{\beta \cos(\theta)} \quad (2)$$

Where k = 0.9 is a dimensionless shape factor, λ_{Cu} depicts the wavelength of Cu-K_α radiation (λ_{Cu} = 1.5406 Å), θ represents the Bragg angle of the most intense peak and β is the full width at half maximum of the Bragg peak. It was 41 nm presented so a nanosized system. This size was a little high due to the method of preparation.

In figure 2(a), we present the Scanning Electron Microscopy (SEM) images of Er_{0.9}Sr_{0.1}Ti_{0.975}Cr_{0.025}O₃ system. It illustrates different shapes of agglomerated grains. The EDS spectrum of the system (figure 2(b)) shows that all chemical elements are present (Er, Sr, Ti, Cr, and O) and there are no strange elements confirming the right composition and no element was lost during sintering [21–23]. Statistical evaluation of the grain size distribution of the studied sample was analyzed via ImageJ software (figure 2(c)). The particle number as a function of the particle size was shown in the same figure. These results were fitted according to Gaussian law to estimate the average particle size which is about 100 nm. Comparing both D_{XRD} and D_{SEM}, we note a difference between the crystallites size obtained from XRD patterns and the particle size extracted from SEM measurement (D_{XRD} < D_{SEM}). This dissimilarity can be attributed to the agglomeration phenomenon and to the fact that each grain of

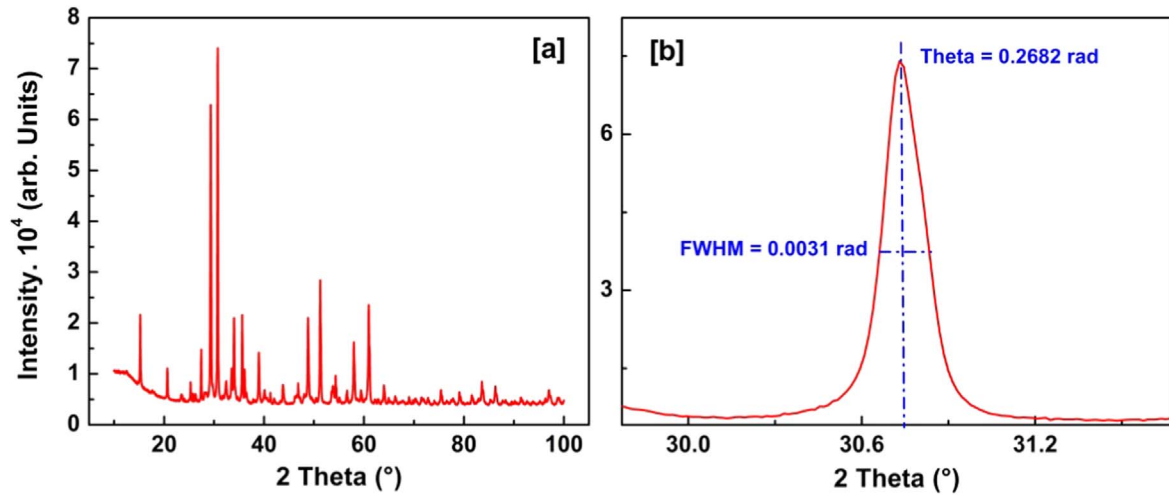


Figure 1. (a), (b): (a) Room temperature powder x-ray diffraction (XRD) pattern of $Er_{0.9}Sr_{0.1}Ti_{0.975}Cr_{0.025}O_3$ system. (b) The enlarged view shows how we determine crystallite size via Debye Scherer's formula.

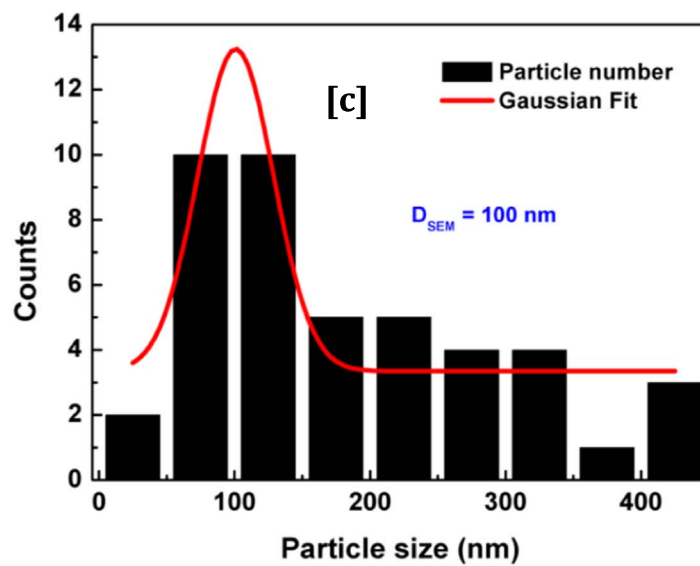
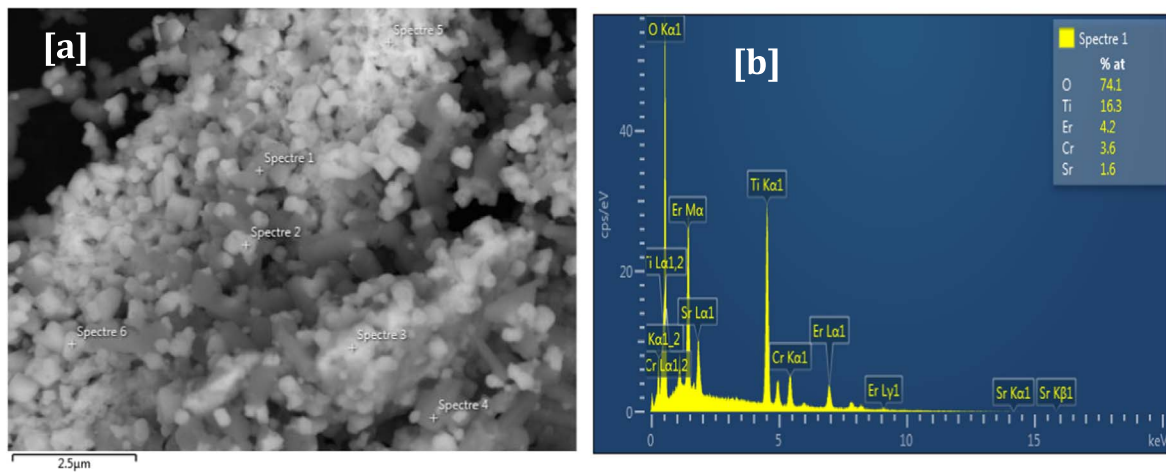


Figure 2. (a)–(c): (a) Scanning Electron Microscopy (SEM), (b) EDS analysis spectrum and (c) the statistical distribution with Gaussian fit of $Er_{0.9}Sr_{0.1}Ti_{0.975}Cr_{0.025}O_3$ system.

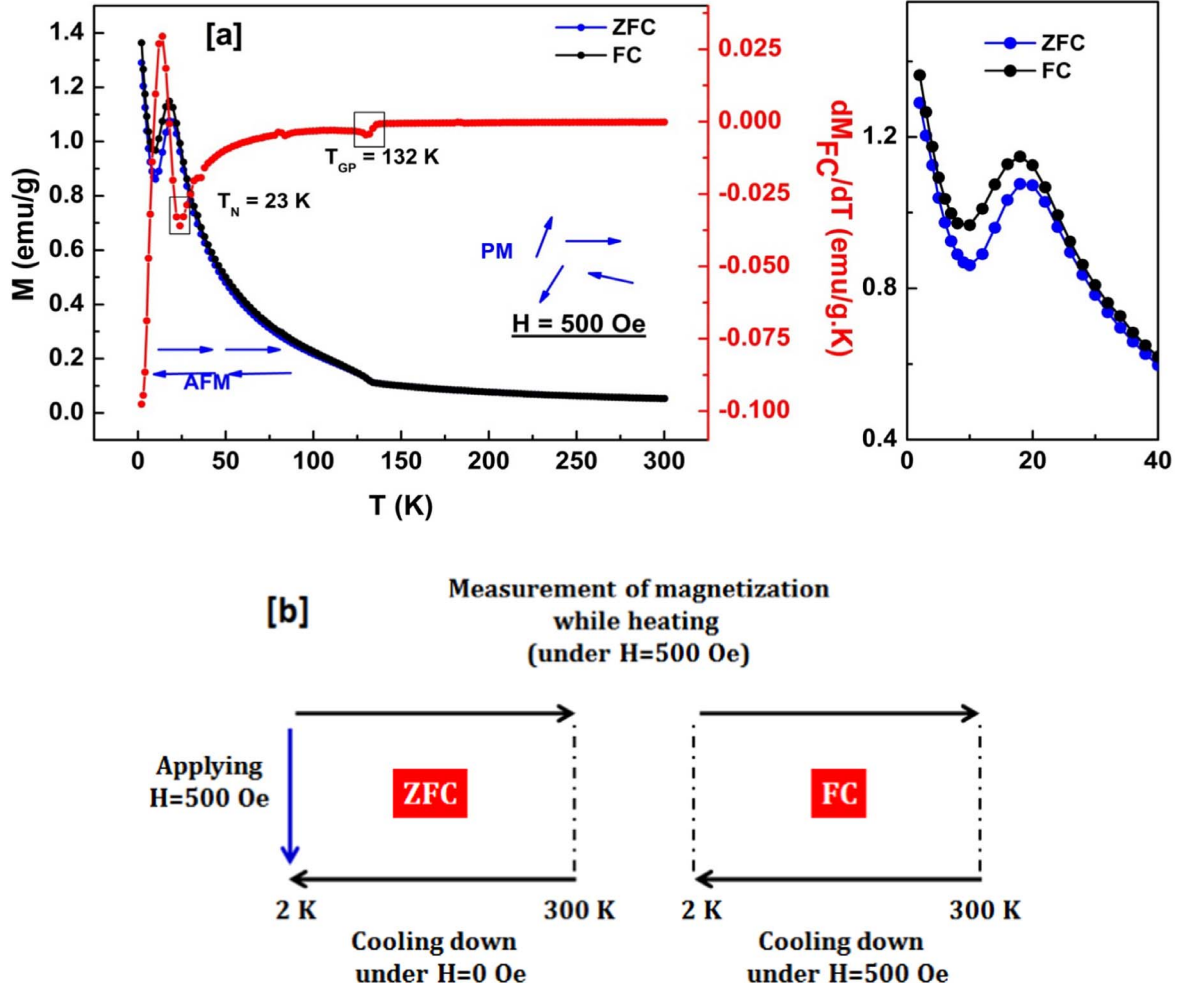


Figure 3. (a), (b): (a) ZFC-FC measurements of $\text{Er}_{0.9}\text{Sr}_{0.1}\text{Ti}_{0.975}\text{Cr}_{0.025}\text{O}_3$ perovskite under 500 Oe and the derivative of M_{FC} versus temperature dM_{FC}/dT . Right-side is an enlarged view to show ZFC-FC plots. (b) ZFC-FC of procedures.

the material is formed by many crystallites [24]. Here, we can define the average agglomeration rate as the ratio of the average particle size by that of crystallite which is around 2.1734.

To understand the magnetic properties of this material, Zero Field Cooled (ZFC) and Field Cooled (FC) modes were performed under 500 Oe magnetic field (figure 3(a)). The procedures of both ZFC/FC measurements are presented in figure 3(b). An important peak appears below 10 K which is related to the arrangement of Er^{3+} magnetic moments as reported by Raneesh *et al* [23]. The minima appearing in the dM/dT plot is corresponding to Neel temperature $T_N = 23$ K.

Thus, the material presents a second-order anti-ferromagnetic-paramagnetic transition (AFM-PM). The minute bifurcation in ZFC-FC measurements was related to the state of non-magnetic Ti^{3+} comparing to Er^{3+} which presents $9.6 \mu_B$ making it PM at high temperatures [23]. It should be marked, then, that the inverse of the molar magnetic susceptibility $1/\chi_m$ of the $\text{Er}_{0.9}\text{Sr}_{0.1}\text{Ti}_{0.975}\text{Cr}_{0.025}\text{O}_3$ system presents a PM phase that can be well fitted to the Curie-Weiss law (C-W) in the PM temperature range figure 4(a). It is

given by this formula:

$$\chi_m = \frac{C_m}{T - \theta_p} \quad (3)$$

Where χ_m is the molar magnetic susceptibility, C_m is the molar Curie constant and θ_p is the Weiss temperature.

The C-W fit provides a negative Weiss temperature $\theta_p = -13.74$ K confirming the dominance of the AFM state at low temperatures. It gives also the $C_m = 8.39$ K. g. $\text{emu}^{-1} \text{mol}^{-1}$ and so the experimental effective moment $\mu_{eff,exp} = 8.16 \mu_B$. The theoretical one is given by (4):

$$\mu_{eff,th} = \sqrt{n_{\text{Er}^{3+}} \mu_{eff}^2(\text{Er}^{3+})} \quad (4)$$

Based on the previous formula, the $\mu_{eff,th} = 9.10 \mu_B$ is not so close to the experimental value suggesting that the PM phase is not fully homogenous [21]. An abrupt downturn starting at 132 K down to 2 K suggests the possibility of existing of Griffiths phase (GP) [25–27]. The Griffiths temperature T_{GP} is the temperature at which the inverse of magnetic susceptibility deviates from C-W law. It is a characteristic temperature for which ferromagnetic (FM) clusters start to be formed; transition temperature [28]. Thus,

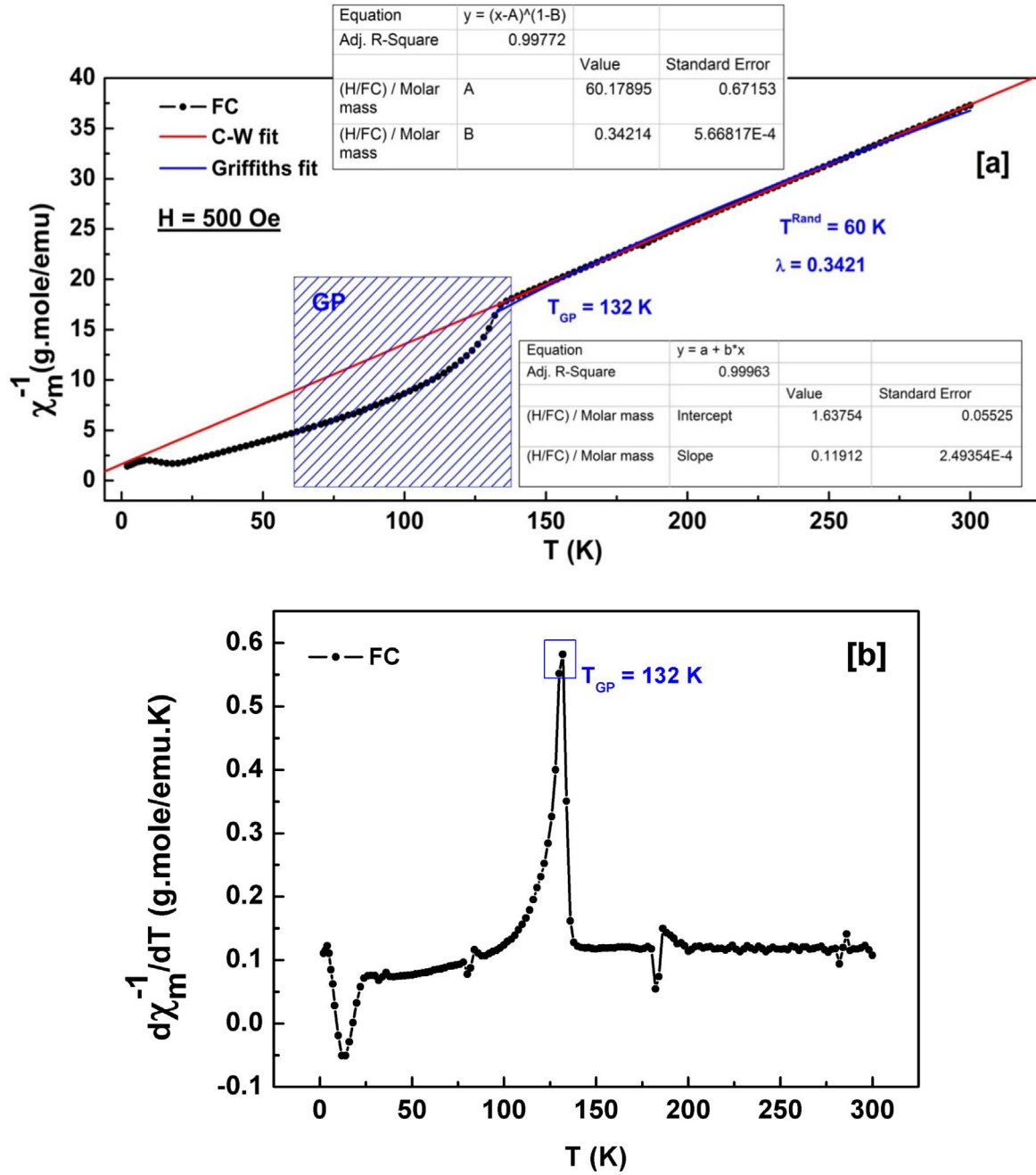


Figure 4. (a), (b): (a) Inverse of molar magnetic susceptibility curves of $\text{Er}_{0.9}\text{Sr}_{0.1}\text{Ti}_{0.975}\text{Cr}_{0.025}\text{O}_3$ Titanate. Straight lines are belonging to Curie-Weiss law (red color) and Griffiths power law (blue color). Hatched surface presents the GP region. (b) The derivative of the inverse of molar magnetic susceptibility versus temperature $d(1/\chi_m)/dT$ to get T_{GP} .

$T_{\text{GP}} = 132$ K which is also illustrated by the dM/dT plot. The T_{GP} can be also determined via $d(1/\chi_m)/dT$ plot as presented in figure 4(b) giving the same value $T_{\text{GP}} = 132$ K. The appearance of Griffiths phase may be due to the presence of short-range spins ferromagnetically correlated above T_{N} ; short-range FM clusters in the PM region in the temperature range $T^{\text{Rand}} \leq T \leq T_{\text{GP}}$, defining Griffiths regime, which can be attributed to the random spatial variation in magnetic exchange interactions due to the nanosized grains [25, 27]. T^{Rand} is the critical temperature of a random FM state where the susceptibility tends to diverge; random transition temperature [28, 29].

The GP is characterized by an exponent λ which is between zero and one, defined by (5):

$$1/\chi_m \propto (T - T^{\text{Rand}})^{1-\lambda} \quad (5)$$

λ means the deviation from to C-W behavior presenting the strength of GP. This power law can be a changed form of the C-W law. Both cases were presented; in the PM regime $\lambda = 0$, so the equation (5) reduces to the formula (3). For non-zero λ , the inverse of magnetic susceptibility follows the equation (5) confirming so the deviation from the C-W law.

Figure 4 (s) shows also the Griffiths fit using power-law formula (5) estimating so the values of both λ and T^{Rand} as

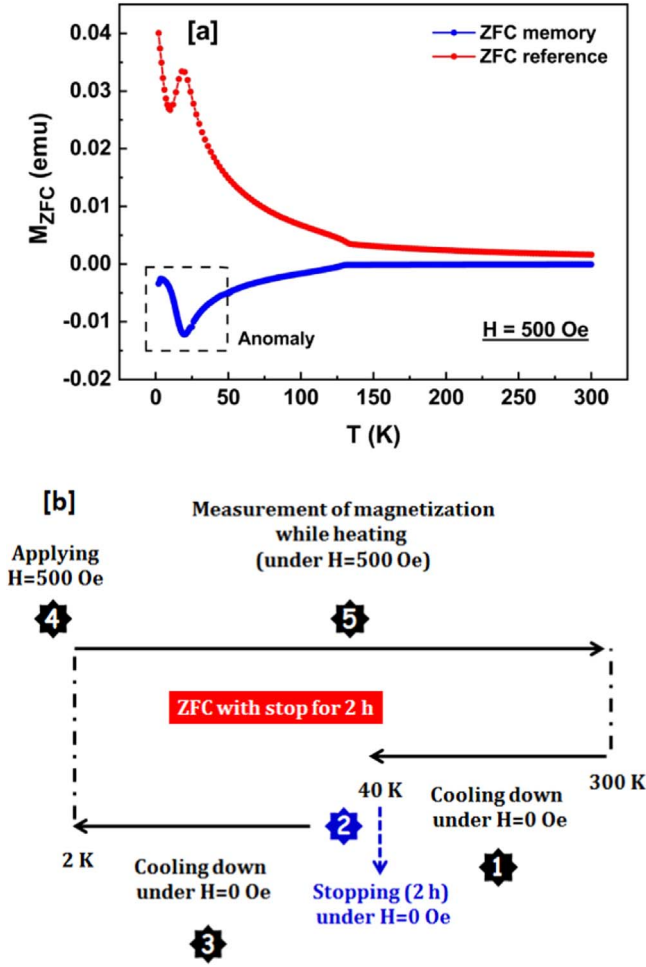


Figure 5. (a), (b): (a) Magnetic memory effect in $\text{Er}_{0.9}\text{Sr}_{0.1}\text{Ti}_{0.975}\text{Cr}_{0.025}\text{O}_3$. (b) Magnetic memory procedure.

$\lambda = 0.3421$ and $T^{\text{Rand}} = 60$ K. Thus, the Griffiths regime is observed in the temperature range of about 72 K ($T_{\text{GP}} - T^{\text{Rand}}$). Such temperature range and λ value indicate that the GP is a little robust comparing to other values in previous works [25, 27–29].

To check the presence of magnetic memory effect in $\text{Er}_{0.9}\text{Sr}_{0.1}\text{Ti}_{0.975}\text{Cr}_{0.025}\text{O}_3$ material, we performed the magnetization measurements in the ZFC mode with an arrest in the characterization for 2 h at 50 K [5, 6] as we present in figure 5(a). The magnetic memory can be employed as a proof of spin-glass state at low temperatures [30]. We note the ZFC measurements in normal conditions as a reference and the stopped one as ZFC memory. The system was cooled from room temperature down to 50 K under 0 Oe with an arrest at 50 K for 2 h where the magnetic field was switched off. After 2 h, the sample was cooled down to 2 K without applying any magnetic field. After reaching 2 K, the sample was warmed up to 300 K under 500 Oe and the memory test was then finished (figure 5(b)). Comparing both plots; we note that the ZFC memory curve presents an anomaly at 50 K presented by a downward started at 50 K down to low temperatures. This illustrates that the sample ‘remembers/memorized’ its thermal history of the stop. The memory effect presented by $\text{Er}_{0.9}\text{Sr}_{0.1}\text{Ti}_{0.975}\text{Cr}_{0.025}\text{O}_3$ system is an obvious signal of

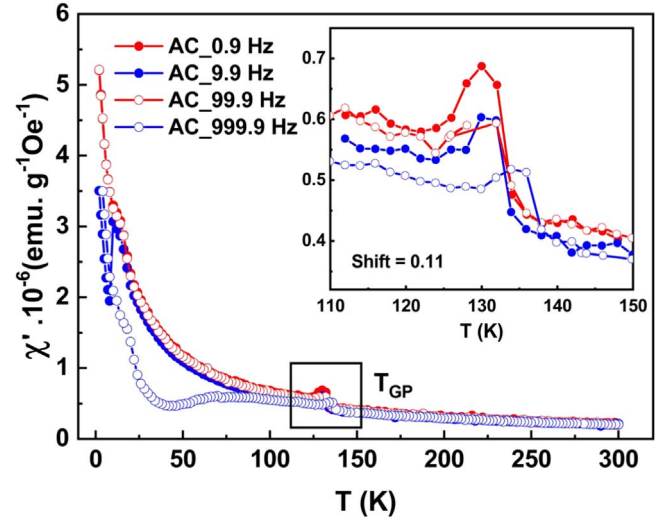


Figure 6. Thermal variation of the in-phase ac-susceptibility (χ') of $\text{Er}_{0.9}\text{Sr}_{0.1}\text{Ti}_{0.975}\text{Cr}_{0.025}\text{O}_3$ titanate for different frequencies 0.9, 9.9, 99.9 and 999.9 Hz. Inset presents zoom around T_{GP} .

spin-glass behavior which is appearing at 50 K. We explain that by the fact that when a sample remains for a period of time (2 h in this case) at one temperature, the major part of the surface magnetic moments is frozen under no applied magnetic field.

A powerful technique for describing materials is called the ac dynamic magnetic susceptibility [31, 32]. It is defined as the differential response of magnetization system to an oscillating magnetic field dM/dH [21]. It is characterized by its susceptibility magnitude χ and its phase shift ϕ . It is used generally to investigate a metastable order [33–36]. The AC susceptibility is a complex value that is given by [33]:

$$\chi = \chi' - i\chi'' \quad (6)$$

With χ' is the in-phase ac susceptibility and χ'' is the imaginary one. They are given by:

$$\chi' = \chi \cos \phi \quad (7)$$

$$\chi'' = \chi \sin \phi \quad (8)$$

$$\chi = \sqrt{\chi'^2 + \chi''^2} \quad (9)$$

$$\phi = \arctan\left(\frac{\chi''}{\chi'}\right) \quad (10)$$

In this work, we have investigated the existence of GP in ac magnetic susceptibility. We present in figure 6 the in-phase ac susceptibility (χ') of $\text{Er}_{0.9}\text{Sr}_{0.1}\text{Ti}_{0.975}\text{Cr}_{0.025}\text{O}_3$ sample at different frequencies 0.9, 9.9, 99.9 and 999.9 Hz. It is clear here the appearance of the GP at T_{GP} as determined by dc susceptibility. The Griffiths phase GP in ac measurements is frequency-dependent as presented by the zoom in the same figure. The anomaly in the inset is shifting towards higher temperatures while increasing the applied frequency. As an example, it varied from 130 K at 0.9 Hz to 135 K at 999.9 Hz; generally, it is quantified by (11):

$$\text{Shift} \propto \frac{\Delta T_{\text{GP}}}{T_{\text{GP}}} \Delta \log(\text{Freq}) \quad (11)$$

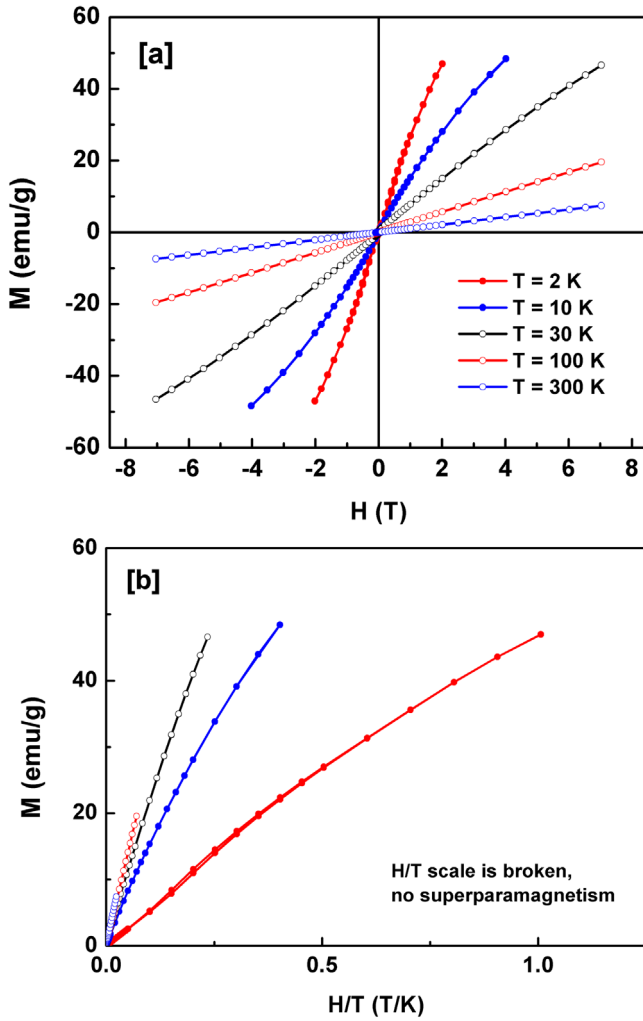


Figure 7. (a), (b): (a) Isothermal magnetization measurements of $\text{Er}_{0.9}\text{Sr}_{0.1}\text{Ti}_{0.975}\text{Cr}_{0.025}\text{O}_3$ measured at 2, 10, 30, 100 and 300 K. (b) M versus H/T plots shows that the scaling fails excluding out the probability of presence of superparamagnetism.

The estimated value in this system is about 0.11, it is more significant than that found in CuMnO_2 by Kaushal *et al* [34] with around 0.003.

Soft magnetic hysteresis loops data (between ± 7 T) of $\text{Er}_{0.9}\text{Sr}_{0.1}\text{Ti}_{0.975}\text{Cr}_{0.025}\text{O}_3$ system (figure 7(a)) depict mostly linear behaviors at 30, 100 and 300 K confirming so the dominance of PM state at high temperatures. For, 2 and 10 K, the M versus H plots are also linear-like lines but they are not straight ones and they do not show any tendency to saturate proving the presence of AFM state at low temperatures [21, 33]. Greedan *et al* [17] in their paper showed that ErTiO_3 saturate at 4.2 K under a low magnetic field. This transformation in the material state is due to the substituting Er by Sr the fact that substituting with Sr dilutes the magnetism [33, 37].

Figure 7(b) shows the break of H/T excluding the existence of a superparamagnetic state (SPM) in the studied sample [35].

Figure 8 (a) presents the isotherms of magnetization $M(H)_{T=\text{const}}$ in the temperature range varying from 2 to 300 K

for various magnetic fields up to 6 T presenting the absence of magnetic hysteresis. These $M(H)_{T=\text{const}}$ isotherms were used as a bridge to determine the magnetic entropy change via Maxwell relation [21, 38]:

$$\Delta S_M(T, \Delta H) = \int_{H_1}^{H_2} \left(\frac{\partial M}{\partial T} \right)_H dH \quad (12)$$

Where H_1 and H_2 are external applied magnetic fields with $\Delta H = H_2 - H_1 \geq 0$.

The isothermal magnetization plots illustrate the presence of more than one magnetic phase versus temperature. Figure 8(b) presents the thermal entropy change ($-\Delta S$) of $\text{Er}_{0.9}\text{Sr}_{0.1}\text{Ti}_{0.975}\text{Cr}_{0.025}\text{O}_3$ system at several magnetic field strengths varying from 1 to 6 T. We remark that the maximum of the entropy change ($-\Delta S_{\text{max}}$) is manifesting at very low temperatures at around 2 K. To determine plainly the ΔS_{max} value and to obtain the RCP values, we choose to fit all the plots to obtain clearly the maximum of the entropy change value via Lorentzian function expressed as follows [39]:

$$L(x) = y_0 + \frac{2A}{\pi} \frac{w}{4(x - x_c)^2 + w^2} \quad (13)$$

With y_0 presents the offset, A shows the area, w is the width of the Lorentzian and x_c is noted as the abscissa of the peak (see the inset of figure 8(b)).

The thermal entropy change ($-\Delta S$) of $\text{Er}_{0.9}\text{Sr}_{0.1}\text{Ti}_{0.975}\text{Cr}_{0.025}\text{O}_3$ is increasing with the external applied magnetic field as presented in the same figure.

We show in figure 8(c) the variation of the RCP parameter versus the applied magnetic field. The titanate-based sample $\text{Er}_{0.9}\text{Sr}_{0.1}\text{Ti}_{0.975}\text{Cr}_{0.025}\text{O}_3$ attains around 292.27 J kg^{-1} at 5 T and 400 J kg^{-1} at 6 T allowing it to be very suitable magnetic refrigerant. These results are lower than those reported by the well-known magnetic refrigerant gadolinium Gd which presents around 410 J kg^{-1} at 5 T, although these RCP values are high enough compared to various other samples. We summarized in table 1 the values of ΔS_{max} and RCP of different materials which are considered as good magnetic refrigerants versus the applied magnetic field.

The specific heat change ΔC_p as a function of temperature is expressed as follows [45, 46]:

$$\Delta C_p(T, \mu_0 H) = -T \frac{\partial \Delta S(T, \mu_0 H)}{\partial T} \quad (14)$$

The thermal variation of the ΔC_p of $\text{Er}_{0.9}\text{Sr}_{0.1}\text{Ti}_{0.975}\text{Cr}_{0.025}\text{O}_3$ system over the temperature range 3–255 K under various magnetic fields from 1 T to 6 T is presented in figure 9.

It is clear here that ΔC_p curves for all applied magnetic fields present negative values. It presents also the same negative peak around very low temperatures as the $-\Delta S$. This peak can affirm the magnetic correlations in this sample [47]. The $\Delta S < 0$ and the $\Delta C_p < 0$; here we can note that the study of specific heat capacity support strongly the magnetocaloric results. We summarized all the magnetocaloric parameters in table 2.

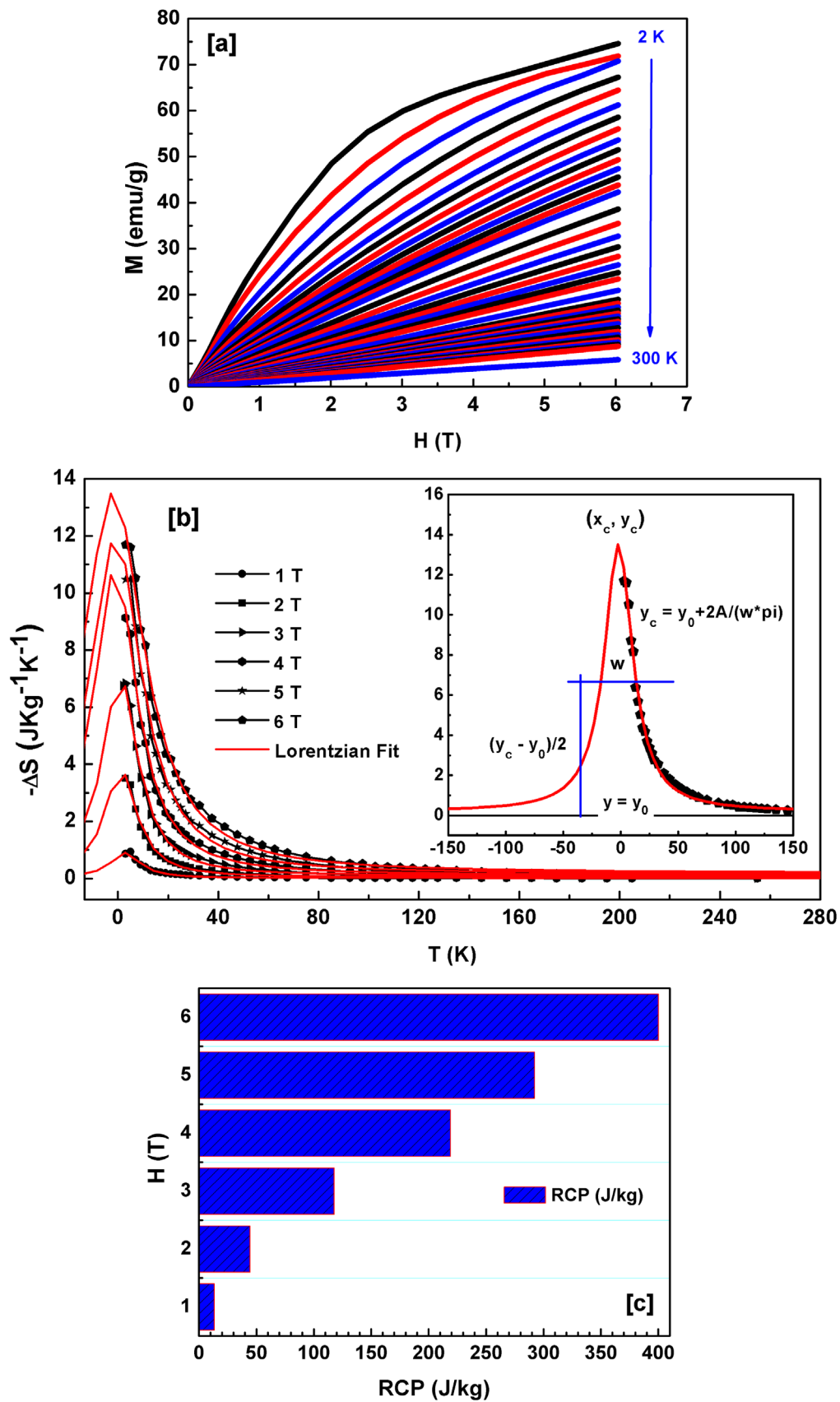


Figure 8. (a)–(c): (a) Magnetization isotherms between 2 to 300 K for a maximum magnetic field of 6 T of $\text{Er}_{0.9}\text{Sr}_{0.1}\text{Ti}_{0.975}\text{Cr}_{0.025}\text{O}_3$ sample. (b) Magnetic entropy change ($-\Delta S$) versus temperature for different magnetic fields ranging from 1 T to 6 T. Red curves are belonging to Lorentzian fit. The inset presents the sample curve explanation when Lorentzian fit is used at 6 T. (c) Relative cooling power (RCP).

Table 1. Comparison of some values of ΔS_{\max} and RCP of different materials versus the applied magnetic fields H.

System	$-\Delta S_{\max}$ [J/(kg K)]	RCP [J/kg]	H (T)	References
$\text{Er}_{0.9}\text{Sr}_{0.1}\text{Ti}_{0.975}\text{Cr}_{0.025}\text{O}_3$	11.61	292.27	5	Present work
$\text{Er}_{0.9}\text{Sr}_{0.1}\text{Ti}_{0.975}\text{Cr}_{0.025}\text{O}_3$	13.41	400.03	6	Present work
$\text{Dy}_{0.5}(\text{Sr}_{0.7}\text{Ca}_{0.3})_{0.5}\text{MnO}_3$	4	169	5	[39]
DyPtGa	6	131.2	5	[40]
Gd	5	196	2	[41]
Gd	10.2	410	5	[42]
$\text{La}_{0.67}\text{Ba}_{0.33}\text{MnO}_3$	1.48	161	5	[43]
$\text{La}_{0.67}\text{Sr}_{0.33}\text{Mn}_{0.9}\text{Cr}_{0.1}\text{O}_3$	2	200	5	[44]

Table 2. Magnetic field dependence of the maximum entropy change ΔS_{\max} , relative cooling power values RCP, the maximum heat capacity $\Delta C_{p-\max}$ and the full width at half maximum δT_{FWHM} of the magnetic entropy change curve.

H (T)	$-\Delta S_{\max}$ [J/(kg K)]	RCP [J/kg]	$\Delta C_{p-\max}$ [J/(kg K)]	δT_{FWHM} (T)
1	0.90	13.47	0.11	15.66
2	3.48	44.5	0.37	17.30
3	6.82	117.68	0.62	18.80
4	10.56	219.09	0.79	22.18
5	11.61	292.27	0.83	26.17
6	13.41	400.03	0.72	30.83

cooling comparing to the most known magnetic refrigerant Gd and many other perovskite materials.

Acknowledgments

The authors would like to acknowledge the contribution of Core Labs group supervised by Dr Said A. Mansour in Qatar Environment and Energy Research Institute, Hamad Bin Khalifa University, Qatar Foundation, especially, Dr Akshath Raghu Shetty for carrying out the XRD measurements.

ORCID iDs

R Hamdi  <https://orcid.org/0000-0002-9364-2664>

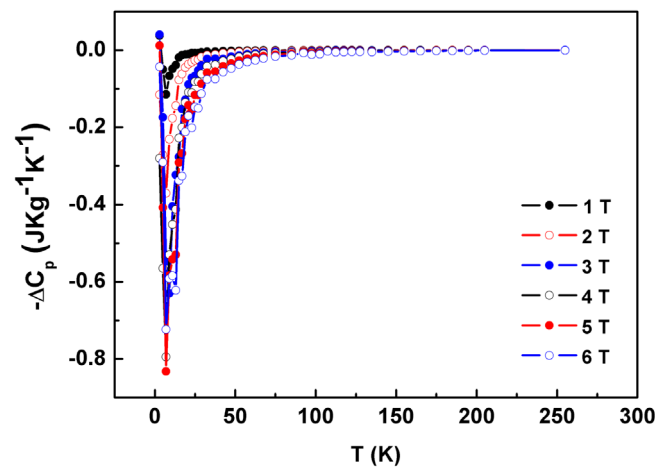
M Smari  <https://orcid.org/0000-0003-0090-3296>

L Bessais  <https://orcid.org/0000-0001-7236-1604>

E Dhahri  <https://orcid.org/0000-0002-6919-8778>

References

- [1] Lanfredi S, Storti F, Simões L P M, Djurado E and Nobre M A L 2017 Synthesis and structural characterization of calcium titanate by spraypyrolysis method *Mater. Lett.* **148–51**
- [2] Bradha M, Vijayaraghavan T, Suriyaraj S P, Selvakumar R and Anuradha Ashok M 2015 Synthesis of photocatalytic $\text{La}(1-x)\text{AxTiO}_{3.5-\delta}$ (A = Ba, Sr, Ca) nano perovskites and their application for photocatalytic oxidation of congo red dye in aqueous solution *J Rare Earth* **33** 2 160
- [3] James M, Avdeev M, Barnes P, Morales L, Wallwork K and Withers R 2007 Orthorhombic superstructures within the rare earth strontium-doped cobaltate perovskites: $\text{Ln}_{1-x}\text{Sr}_x\text{CoO}_{3-\delta}$ (Ln = Y3+, Dy3+ -Yb3+; $0.750 \leq x \leq 0.875$) *J. Solid State Chem.* **180** 2233
- [4] Deng Z Q, Liu W, Peng D K, Chen C and Sand Yang W S 2004 Combustion synthesis, annealing, and oxygen permeation properties of $\text{SrFeCo}_{0.5}\text{O}_y$ membranes *Mater. Res. Bull.* **39** 963–9
- [5] Ghosh N, Datta S and Ghosh B 2015 Size dependence in magnetic memory, relaxation and interaction of $\text{La}_{0.67}\text{Sr}_{0.33}\text{MnO}_3$ *J. Magn. Magn. Mater.* **382** 277
- [6] Hamdi R, Tozri A, Smari M, Dhahri E and Bessais L 2017 Resistivity, I–V characteristics and Hall effect in $\text{Dy}_{0.5}(\text{Sr}_{1-x}\text{Ca}_x)_{0.5}\text{MnO}_3$ manganites *Mater. Res. Bull.* **95** 525–31

**Figure 9.** Thermal variation of the specific heat ΔC_p of $\text{Er}_{0.9}\text{Sr}_{0.1}\text{Ti}_{0.975}\text{Cr}_{0.025}\text{O}_3$ sample under various magnetic fields from 1 T to 6 T.

4. Conclusion

$\text{Er}_{0.9}\text{Sr}_{0.1}\text{Ti}_{0.975}\text{Cr}_{0.025}\text{O}_3$ nanomaterial presents a cubic structure with $Fd-3m$ (227) as a space group. Based on magnetic measurements, it presents a second order anti-ferromagnetic transition. It illustrates also the existence of Griffiths phase at around $T_{\text{GP}} = 132$ K. Magnetic memory exists in this system; it remembers its thermal history. Relative cooling power of this sample is around 292.27 J kg^{-1} at 5 T and 400 J kg^{-1} at 6 T making it suitable for magnetic

- [7] Daivajna M D, Rao A and Okram G S 2015 Electrical, thermal and magnetic studies on Bi-substituted LSMO manganites *J. Magn. Magn. Mater.* **388** 90–5
- [8] Hamdi R, Tozri A, Dhahri E and Bessais L 2017 Brilliant effect of Ca substitution in the appearance of magnetic memory in $\text{Dy}_{0.5}(\text{Sr}_{1-x}\text{Ca}_x)_0.5\text{MnO}_3$ ($x = 0.3$) manganites *Intermetallics* **89** 118–22
- [9] Vadnala S, Durga Rao T, Prem P and Asthana S 2014 Enhancement of magnetic and electrical properties in Sc substituted BiFeO_3 multiferroic *Physica B* **448** 277–80
- [10] Smari M, Hamouda R, Walha I, Dhahri E, Mompeán F J and Hernández M G 2015 Magnetic and magnetoresistance in half-doped manganite $\text{La}_{0.5}\text{Ca}_{0.5}\text{MnO}_3$ and $\text{La}_{0.5}\text{Ca}_{0.4}\text{Ag}_{0.1}\text{MnO}_3$ *J Alloy Compd.* **644** 632–7
- [11] Yang X S, Yang L Q, Cheng C H, Lv L and Zhao Y 2012 Magnetoresistance, electroresistance and nonlinear electrical behavior in nanopolycrystalline $\text{La}_2/3\text{Sr}_{1/3}\text{MnO}_3$ *Phys. Procedia* **27** 96–9
- [12] Smari M, Walha I, Dhahri E and Hlil E K 2014 Collapse of charge ordering and enhancement of magnetocaloric effect in $\text{La}_{0.5}\text{Ca}_{0.5-x}\text{Ag}_x\text{MnO}_3$ ($x = 0.0$ and 0.2) *Chem. Phys. Lett.* **607** 25–8
- [13] Tozri A, Dhahri E and Hlil E K 2010 Magnetic transition and magnetic entropy changes of $\text{La}_{0.8}\text{Pb}_{0.1}\text{MnO}_3$ and $\text{La}_{0.8}\text{Pb}_{0.1}\text{Na}_{0.1}\text{MnO}_3$ *Mater. Lett.* **64** 2138–41
- [14] Tozri A, Dhahri E, Hlil E K and Valente M A 2011 Critical behavior near the paramagnetic to ferromagnetic phase transition temperature in $\text{La}_{0.7}\text{Pb}_{0.05}\text{Na}_{0.25}\text{MnO}_3$ *Solid State Commun.* **151** 315–20
- [15] Sale A G, Kazan S, Gatiatova Ju I, Valeev V F, Khaibullin R I and Mikailzade F A 2013 Magnetic properties of Fe implanted SrTiO_3 perovskite crystal *Mater. Res. Bull.* **48** 2861–4
- [16] Bannikov V V, Shein I R, Kozhevnikov V L and Ivanovskii A L 2008 Magnetism without magnetic ions in non-magnetic perovskites SrTiO_3 , SrZrO_3 and SrSnO_3 *J. Magn. Magn. Mater.* **320** 936–42
- [17] Greedan J E, Carl Turner W and Goodings D A 1984 Magnetization and magnetic susceptibility of single crystals of HoTiO_3 and ErTiO_3 *J. Magn. Magn. Mater.* **42** 255–62
- [18] Dhara S, Roy Chowdhury R and Bandyopadhyay B 2015 Strong memory effect at room temperature in nanostructured granular alloy $\text{Co}_{0.3}\text{Cu}_{0.7}$ *RSC Adv.* **5** 95695
- [19] Sun Y, Salamon M B, Garnier K and Averbach R S 2003 Memory effects in an interacting magnetic nanoparticle system *Phys. Rev. Lett.* **91** 167206
- [20] Khlifi M, Dhahri E and Hlil E K 2014 Scaling laws for the magnetocaloric effect in calcium deficiency manganites $\text{La}_{0.8}\text{Ca}_{0.2-xx}\text{MnO}_3$ with a second-order magnetic phase transition *J. Super. Nov. Magn.* **27** 1341–5
- [21] Hamdi R, Tozri A, Smari M, Dhahri E and Bessais L 2017 Structural, magnetic, magnetocaloric and electrical studies of $\text{Dy}_{0.5}(\text{Sr}_{1-x}\text{Ca}_x)_0.5\text{MnO}_3$ manganites *J. Magn. Magn. Mater.* **444** 270–9
- [22] Tozri A, Dhahri E and Hlil E K 2010 Effects of vacancy and Na doping on the structural, magnetic and transport properties of $\text{La}_{0.8}\text{Pb}_{0.1}(\square/\text{Na})_0.1\text{MnO}_3$ *J. Magn. Magn. Mater.* **322** 2516–24
- [23] Raneesh B, Saha A, Das D and Kalarikkal N 2013 Structural and magnetic properties of geometrically frustrated multiferroic ErMnO_3 nanoparticles *J. Alloys Compd.* **551** 654–9
- [24] Chouaya H, Smari M, Walha I, Dhahri E, Graça M P F and Valente M A 2018 The effect of bismuth on the structure, magnetic and electric properties of Co_2MnO_4 spinel multiferroic *J. Magn. Magn. Mater.* **451** 344–50
- [25] Karmakar A, Majumdar S, Kundu S and Nath T K 2012 Observation of Griffiths phase in antiferromagnetic $\text{La}_{0.32}\text{Eu}_{0.68}\text{MnO}_3$ *J. Phys. Condens. Matter* **24** 126003
- [26] Griffiths R B 1969 Nonanalytic behavior above the critical point in a random ising ferromagnet *Phys. Rev. Lett.* **23** 17
- [27] Baaziz H, Tozri A, Dhahri E and Hlil E K 2016 Size-induced Griffiths phase-like in ferromagnetic metallic $\text{La}_{0.67}\text{Sr}_{0.33}\text{MnO}_3$ nanoparticles *J. Magn. Magn. Mater.* **403** 181–7
- [28] Sanjib B, Nasrin B and Das I 2018 Evolution from non-Griffiths phase to Griffiths phase: giant enhancement of magnetoresistance in nanocrystalline $(\text{La}_{0.4}\text{Y}_{0.6})_{0.7}\text{Ca}_{0.3}\text{MnO}_3$ compound *J. Alloys Compd.* **745** 753–760
- [29] Wanjun J, XueZhi Z, Gwyn W, Mukovskii Y and Privezentsev R 2010 Coexistence of colossal magnetoresistance, a Griffiths-like phase, and a ferromagnetic insulating ground state in single crystal $\text{La}_{0.73}\text{Ba}_{0.27}\text{MnO}_3$ *J. Appl. Phys.* **107** 09D701
- [30] Shi X M, Ouyang Z W, Ruan M Y, Guo Y M, Cheng J J and Xia Z C 2014 Memory effect and magnetic relaxation in $\text{Ca}_3\text{Co}_2\text{O}_6$ and the doped compounds *Physica B* **433** 21–7
- [31] Bałanda M 2013 AC susceptibility studies of phase transitions and magnetic relaxation: conventional, molecular and low-dimensional magnets *Acta Phys. Pol. A* **124**
- [32] Chen C, He L, Leng Y and Li X 2009 Weak ferromagnetism and spin-glass state with nanosized nickel carbide *J. Appl. Phys.* **105** 123923
- [33] Hamdi R, Tozri A, Smari M, Nouri K, Dhahri E and Bessais L 2019 Structural, magnetic and AC susceptibility properties of $\text{Dy}_{0.5}(\text{Sr}_{1-x}\text{Ca}_x)_0.5\text{MnO}_3$ ($0 < x < 0.3$) manganites *J. Mol. Struct.* **1175** 844–51
- [34] Kaushal Shukla K, Rahul S, Kumar A, Ghosh A K and Sandip C 2017 Griffith-like phase in Crednerite CuMnO_2 *Mater. Res. Bull.* **91** 135–9
- [35] Harikrishnan S, Naveen Kumar C M, Bhat H L, Elizabeth S, Röbber U K, Dörr K, Röbber S and Wirth S 2008 Investigations on the spin-glass state in $\text{Dy}_{0.5}\text{Sr}_{0.5}\text{MnO}_3$ single crystals through structural, magnetic and thermal properties *J. Phys. Condens. Matter* **20** 275234
- [36] Chen D X, Skumryev V and Bozzo B 2011 Calibration of ac and dc magnetometers with a Dy_2O_3 standard *Rev. Sci. Instrum.* **82** 045112
- [37] Röbber S, Harikrishnan S, Röbber U K, Elizabeth S, Bhat H L, Steglich F and Wirth S 2010 Interacting magnetic sublattices and ferrimagnetism in Sr-doped DyMnO_3 *J. Phys. Conf. Series* **200** 012168
- [38] Smari M, Walha I, Dhahri E and Hlil E K 2013 Structural, magnetic and magnetocaloric properties of Ag-doped $\text{La}_{0.5}\text{Ca}_{0.5-x}\text{Ag}_x\text{MnO}_3$ compounds with $0 \leq x \leq 0.4$ *J. Alloys Compd.* **579** 564–71
- [39] Hamdi R, Tozri A, Dhahri E and Bessais L 2017 Magnetocaloric properties and Landau theory of $\text{Dy}_{0.5}(\text{Sr}_{1-x}\text{Ca}_x)_0.5\text{MnO}_3$ ($0 \leq x \leq 0.3$) manganites at cryogenic temperatures *Chem. Phys. Lett.* **680** 94–100
- [40] França E L T, Dos Santos A O, Coelho A A and Da Silva L M 2016 Magnetocaloric effect of the ternary Dy, Ho and Er platinum gallides *J. Magn. Magn. Mater.* **401** 1088–92
- [41] Pecharsky V K and Gschneidner K A 1997 Giant magnetocaloric effect in $\text{Gd}_5(\text{Si}_2\text{Ge}_2)$ *J. Phys. Rev. Lett.* **78** 4494
- [42] Phan M H and Yu S C 2007 Review of the magnetocaloric effect in manganite materials *J. Magn. Magn. Mater.* **308** 325
- [43] Morelli D T, Mance A M, Mantese J V and Micheli A L 1996 Magnetocaloric properties of doped lanthanum manganite films *J. Appl. Phys.* **79** 373
- [44] Sun Y, Tong W and Zhang Y H 2001 Large magnetic entropy change above 300 K in $\text{La}_{0.67}\text{Sr}_{0.33}\text{Mn}_{0.9}\text{Cr}_{0.1}\text{O}_3$ *J. Magn. Magn. Mater.* **232** 205
- [45] Abassi M, Dhahri N, Dhahri J and Hlil E K 2014 Structural and large magnetocaloric properties of

- La_{0.67-x}Y_xBa_{0.23}Ca_{0.1}MnO₃ perovskites
(0 ≤ x ≤ 0.15) *Physica B* **449** 138–43
- [46] Tlili R, Omri A, Bejar M, Dhahri E and Hlil E K 2015 Theoretical investigation of the magnetocaloric effect of La_{0.7}(Ba, Sr)_{0.3}MnO₃ compound at room temperature with a second-order magnetic phase transition *Ceram. Int.* **41** 10654–8
- [47] Kamel R, Tozri A, Dhahri E, Hlil E K and Bessais L 2017 Structural and magnetic studies on perovskite rare-earth manganites(Nd_{1-x}Gd_x)_{0.55}Sr_{0.45}MnO₃(x = 0, 0.1, 0.3 and 0.5): observation of two-step magnetization and negative magnetization behavior *J. Magn. Magn. Mater.* **426** 757–66